BROOKHAVEN
NATIONAL LABORATORY

BNL-211777-2019-JAAM

Low-Temperature Charging Dynamics of the Ionic Liquid and Its Gating Effect on FeSe0.5Te0.5 Superconducting Films

C. Zhang, Q. Li

To be published in "ACS APPLIED MATERIALS & INTERFACES"

May 2019

Condensed Matter Physics and Materials Science Department
Brookhaven National Laboratory

U.S. Department of Energy
USDOE Office of Science (SC), Basic Energy Sciences (BES) (SC-22)

Notice: This manuscript has been authored by employees of Brookhaven Science Associates, LLC under Contract No. DE-SC0012704 with the U.S. Department of Energy. The publisher by accepting the manuscript for publication acknowledges that the United States Government retains a non-exclusive, paid-up, irrevocable, world-wide license to publish or reproduce the published form of this manuscript, or allow others to do so, for United States Government purposes.

DISCLAIMER

This report was prepared as an account of work sponsored by an agency of the United States Government. Neither the United States Government nor any agency thereof, nor any of their employees, nor any of their contractors, subcontractors, or their employees, makes any warranty, express or implied, or assumes any legal liability or responsibility for the accuracy, completeness, or any third party's use or the results of such use of any information, apparatus, product, or process disclosed, or represents that its use would not infringe privately owned rights. Reference herein to any specific commercial product, process, or service by trade name, trademark, manufacturer, or otherwise, does not necessarily constitute or imply its endorsement, recommendation, or favoring by the United States Government or any agency thereof or its contractors or subcontractors. The views and opinions of authors expressed herein do not necessarily state or reflect those of the United States Government or any agency thereof.

Low Temperature Charging Dynamics of Ionic Liquid and Its Gating Effect on $FeSe_{0.5}Te_{0.5}$ Superconducting Films

Cheng Zhang[1,2], Wei Zhao[3], Sheng Bi[3], Christopher M. Rouleau[2], Jason D. Fowlkes[2], Walker Boldman[1], Genda Gu[4], Qiang Li[4], Guang Feng[3], and Philip D. Rack[1,2,]*

[1] Department of Materials Science and Engineering, University of Tennessee, Knoxville, Tennessee 37996, USA

[2] Center for Nanophase Materials Sciences, Oak Ridge National Laboratory, Oak Ridge, Tennessee 37831, USA

[3] State Key Laboratory of Coal Combustion, School of Energy and Power Engineering, Huazhong University of Science and Technology (HUST), Wuhan 430074, China

[4] Department of Condensed Matter Physics and Materials Science, Brookhaven National Laboratory, Upton, New York 11973, USA

***prack@utk.edu**

Abstract

Ionic liquids (IL) have been investigated extensively to electrostatically dope materials to high carrier concentrations. To accomplish this, an electric double layer (EDL) is formed at the interface of the IL and the material channel, which induces a very high electrical field. Electrochemical etching on the IL-channel interface has also been reported and thus for certain materials low temperature IL charging is needed to limit the etching kinetics. While many experiments have been demonstrated in the literature, very little is understood about the low temperature charging dynamics which can have profound effects on the EDL. Here we report our investigation of the low temperature (~210 K) charging dynamics in two widely used ILs – DEME-TF_2N and C_4mim-TF_2N. The results show that the formation of the EDL at low temperature requires a long time and an equivalent voltage V_e is introduced as a measure of the EDL formation during the biasing process. The experimental observation is supported by molecular dynamic simulation, which show that the dynamics are logically a function of gate voltage, time and temperature. To demonstrate the importance of understanding the charging dynamics, a 140 nm thick $FeSe_{0.5}Te_{0.5}$ film was biased using the DEME IL and its onset T_c can be tuned from 18 to a maximum of 35 K for $0 \leq V_e \leq 2.16$ V; when $V_e > 2.16$ V T_c systematically decreases as apparently the superconductor becomes over-doped.

Introduction

Ionic liquids (IL) have been investigated extensively for their unique ability to form an electric double layer (EDL) at relatively low operating voltages.[1-4] When an external voltage is applied on the liquid, cations and anions are oriented to form an EDL at the IL-channel interface and support high electrical fields, which has been widely used to electrostatically gate carrier densities in field-effect transistors. [5-9] It has also been used to extract and intercalate oxygen anions in oxide materials such as TiO_2, $SrTiO_3$ and MoO_3.[6, 10-14] Recently, investigations of the electrostatic doping on superconducting materials has also been studied. Though the detailed underlying mechanism is not completely understood yet, it has been found in different superconductors that appropriate carrier doping can enhance the superconducting transition temperature (T_c).[4, 15-23] N,N-dethyl-N-methyl-N-(2-methoxyethyl)ammonium bis(trifluoromethanesulphonyl)imide, known as DEME-TF_2N, is one of the commonly used IL and demonstrated to work on both cuprate and iron-based superconductors to enhance T_c. However it has also been noted that electrochemical etching can occur at certain voltage/temperature regimes for some IL-superconducting materials combinations[20, 22]. One of the ways to avoid etching is to perform gate biasing at low temperature, typically 220 K, which is just slightly higher than the DEME IL glass transition temperature (~200 K). While electrochemical etching can be minimized at low temperature, ion migration rates and thus the EDL formation is also slower. To our knowledge, the low temperature dynamics of EDL formation has not been carefully studied, which is critical to understand as slow EDL formation times can confuse the interpretation of low temperature electrostatic doping studies.

In this report we present our study of low temperature charging dynamics of two ILs, DEME-TF_2N and C_4mim-TF_2N. The C_4mim-TF_2N IL, also known as Bmim-TF_2N, has been commonly used in recent semiconductor gating studies. Based on these results, the gating effect on $FeSe_{0.5}Te_{0.5}$ (FST) thin films with the DEME IL is also investigated. FST belongs to the "11" type iron-based superconductor, which has the simplest structure and lowest toxicity in the iron-based family. However, these iron chalcogenides have lower T_c compare to iron arsenides. Thus, strategies have been studied to enhance its T_c through different processing techniques, such as oxygen annealing and ion irradiation.[24-26] IL gating has also been studied on iron chalcogenides. Hanzawa *et al* reported an investigation on FeSe thin films and showed that the onset superconducting transition temperature (T_c^{on}) can be enhanced from ~8 K to 35 K by applying V_g = 5.5 V to the DEME IL gate.[16] They found that the enhancement is realized on ~10 nm thick FeSe films, but not on those with 100 nm thickness. A similar study was done by Shiogai *et al*, where it was demonstrated that T_c of FeSe films can be enhanced by IL gating after electrochemical etching/thinning of the films.[20] FeSe in the form of exfoliated flakes has also been studied by Lei *et al*, where they used both IL gating and solid dielectric gating to enhanced the T_c^{on} to an even higher temperature (~45 K).[17, 18] However, we are not aware of any studies showing IL T_c enhancement on the FST material in any form. FST has a zero resistance superconducting transition temperature (T_c^0) of ~14 K for bulk crystals and > 16 K in the thin film form.[27-29] Our previous reports has shown its T_c^0 can be further enhanced to ~18 K by using a CeO_2 buffer layer.[30, 31] Thus we investigated whether IL gating can enhance the superconducting properties of FST thin films, which intrinsically has a higher T_c than FeSe.

Experimental Methods

Ionic Liquid Test. DEME-TF_2N IL was purchased from Sigma-Aldrich. Low temperature dynamic tests were conducted using copper tape as the substrate. A ground wire was connected on the copper using silver paint. Various size IL droplets were put on the copper tape and gate electrodes were made with silver epoxy, which was subsequently suspended on the liquid (Fig. 2a). The sample was put into a Quantum Design Physics Property Measurement System (PPMS) to conduct electrical measurements. Two Keithly 2400 sources were used to apply gate voltages V_g = 3 V and 5 V at 220 K while the gate current I_g was monitored for up to 3 hours. During the low temperature biasing, an equivalent gate voltage V_e was periodically determined by lowering the applied V_g in 0.01 V steps until $I_g < 0.1$ nA (and typically switched polarity to negative current).

Molecular Dynamics Simulation. Figure 4a shows the MD system which consists a slab of room temperature IL [C_4mim][Tf_2N] enclosed between Ag (111) and Cu (111) electrodes. The electrodes have an area of 6.0×6.0 nm^2 in the xy-plane and were separated by 8.0 nm in z-direction, which is wide enough to produce a bulk-like IL region in the middle of system. The gate voltage applied between electrodes was maintained using the constant potential method (CPM) during the simulation,[32] since CPM could correctly mimic the charging process.[33] The electrode potential was applied on a plane across the center of surface atoms, and the number of ion pairs inside the channel was tuned to ensure the ILs in central part of the channel maintaining a bulk-like state. An all-atom model was adopted for the IL [C_4mim][Tf_2N],[34] and the force fields for the electrodes were taken from Ref. [35], which can render accurate interfacial properties at face-centered cubic metal surface. Through the implementation of CPM, MD simulations were performed via a customized GROMACS code in the canonical ensemble,[36] with a time step of 2 fs. The chemical bonds including H-atom in RTILs were constrained by linear constraint solver (LINCS) algorithm.[37] Three different temperatures of ILs (400, 300 and 210 K) were coupled with the velocity re-scaling thermostat.[38] The electrostatic interactions were computed using the PME method[39] with an FFT grid spacing of 0.1 nm and cubic interpolation for charge distribution. The cutoffs for both Coulombic and van der Waals interactions are 1.2 nm. Each simulation was first run for 10 ns to reach equilibrium, and then an 80 ns production run was performed for analysis. To ensure the accuracy of the charging process data, each case was repeated ten times with different initial configurations for analysis.

$FeSe_{0.5}Te_{0.5}$ Superconducting Film Test. FST thin films were epitaxially grown on single crystalline yttrium stabilized zirconia oxide (YSZ) substrate, with a CeO_2 buffer layer. The detailed growth conditions can be found in our previous reports.[25, 31, 40] In-line-4-point contacts were made on the film surface using silver paint and gold wires. The film was then covered by GE varnish, leaving a 0.4 mm by 0.5 mm hole between two voltage leads to act as a reservoir/well for contact with the IL (Fig. 6a). The 4-point probe FST film was then measured in the PPMS after various V_g holding times to establish various V_e. Multiple steps/times of electrostatic biasing were performed at 220 K with V_g = 3 V. After each gate biasing step, the sample was cooled down to 5 K and the resistance versus temperature (RT) curve was measured by warming up to 220 K. V_e for each measured curve was measured, as described above, after the temperature reached 220 K. Notably, V_e is stable during the temperature drop and RT curve measurement as the IL drops below glass transition temperature. T_c^0 is determined by the temperature at which the resistance reached 1% of

its normal state resistance. T_c^{on} is determined by the intersection of the extrapolated normal state RT curve and the linearly fitted superconducting transition region of the RT curve (Fig. S5). Focused ion beam (FIB) milling and subsequent imaging was conducted using FEI 600 Nova dual scanning electron/ion microscope (SEM) to mill the pristine and biased film, to monitor any electrochemical etching during IL biasing. High-resolution cross-sectional secondary electron images and energy dispersive x-ray spectroscopy line scans were taken using a Zeiss Merlin SEM.

Result and discussion

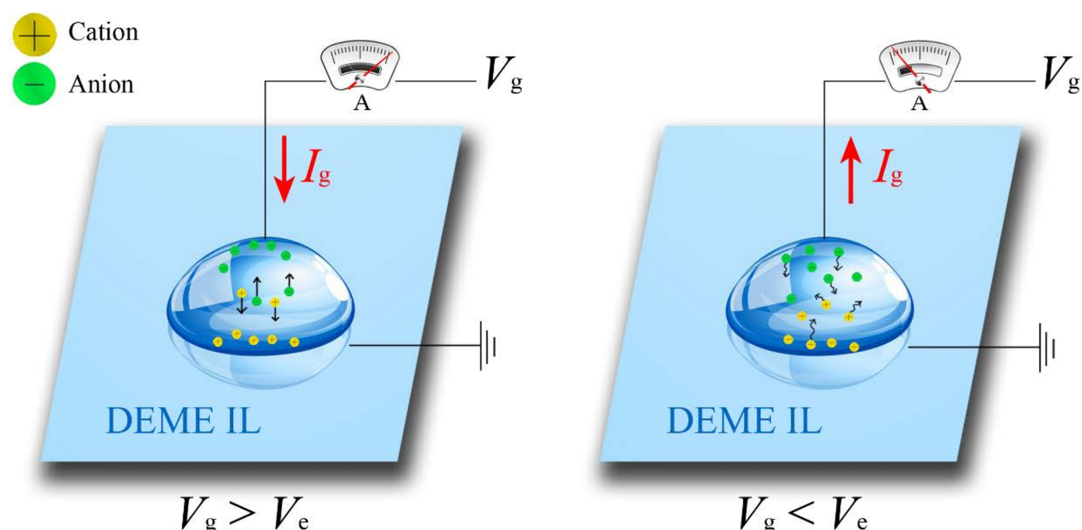

Figure 1. Schematic of low temperature electrical double layer dynamics of DEME-TF$_2$N ionic liquid under positive gate bias. When $V_g > V_e$, current flows during the formation of the EDL (left panel); to measure the V_e of the EDL the gate voltage is incrementally lowered until the applied V_g drops below V_e. At this point the current drops below 0.1nA (and changes polarity), which is interpreted as ion migration from the EDL layer and a decrease in the ion concentration in the EDL (right panel).

Ions inside the pristine IL before bias are randomly distributed. Once a positive V_g is applied, cations and anions migrate to form an EDL on the anode and cathode, respectively. Similar to charging a capacitor, during this IL charging process a current flow, I_g, is detected due to the migration of the ions. Once the EDL saturates I_g becomes zero. If V_g is then released to zero, the oriented ions will tend to move back to an equilibrium state due to their mutual Coulomb repulsion. This charging and releasing process happens very fast at room temperature; however, at low temperature longer time is needed due to the low ion migration rates at higher viscosity. To understand the EDL dynamics at low temperature we introduce an equivalent voltage V_e. It is defined as the value of applied external $V_{g,}$ in which I_g drops below 0.1 nA or slightly switches polarity, and thus represents a pseudo-saturated state of the EDL. For example, if biasing at $V_g = 5$ V as a function of time, V_e will start at 0 V, and increases toward 5 V as the ions migrate to each electrode. Importantly, the dynamics of V_e as a function of time is strongly temperature dependent. To measure the V_e at a certain time during the biasing process, we lower the external applied V_g until $I_g < 0.1$nA. Under this scheme, when $V_g > V_e$, charging occurs and a positive current flow will be detected, and vice versa. Figure 1 schematically illustrates the EDL charging (left panel) and de-charging (right panel) when $V_g > V_e$

and $V_g < V_e$, respectively.

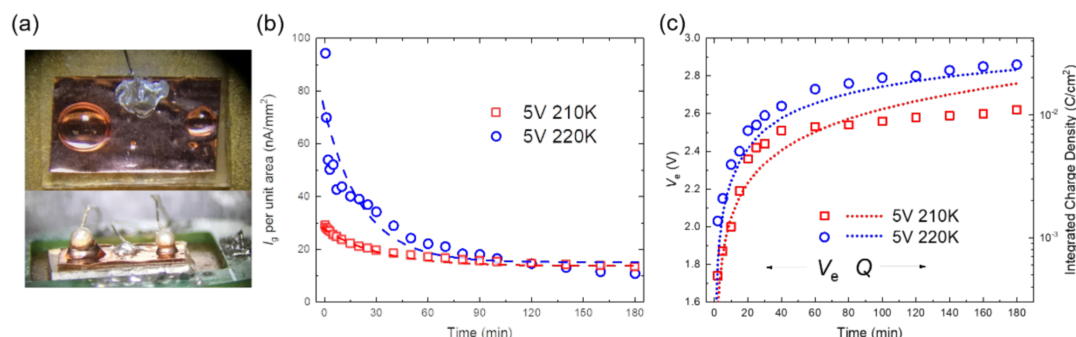

Figure 2. Time dependent gate current (I_g) and equivalent voltage (V_e) in DEME IL with an applied gate voltage of 5 V, measured at 210 K and 220 K. A typical sample set-up for the measurement is shown in (a). Droplets with varies of sizes were tested and the current density, normalized based on the droplet projected area, as a function of time is plotted in (b), dash lines are exponential decay fittings $I_g = A\exp(x/t) + B$. The measured V_e as a function of time is shown in (c) (red squares and blue circles, left axis); note that the integrated charge density increases logarithmically (dotted lines, right axis), V_e increases much slower.

To understand the low temperature charging dynamics of DEME IL, the time dependent I_g and V_e were measured for different size IL droplets. Figure 2b shows the plot of normalized current density as a function of time under 5 V constant gate biasing, measured at 220 K and 210 K. As expected higher temperature results in larger average current flow, and both experience an exponential decay, as shown in fitted dash lines in Figure 2b, in the accumulation of the EDL ion density. To confirm this, we also measured V_e, as described above, as a function of time. Figure 2c illustrates the time dependence of V_e (left axis) compared to the integrated charge density (right axis, log scale), which both show the dynamics of the EDL layer formation. The accumulated charge density was calculated from Figure 2b by integrating I_g over time, based on the assumption that all charge is accumulated in the EDL. Interestingly the charging rate increases logarithmically whereas the effective voltage increases on a more linear scale. We attribute this to the fact that multiple ion layers are accumulating and ions accumulating farther from the IL/anode interface contribute less to the effective voltage/field in the material. Another test with 3 V biasing at two temperatures was conducted and the result is shown in Figure 3a,b. As expected, the V_e increases slower at a lower voltage, however after 180 minutes at 220 K V_e only reaches 2.55 V, which is a higher fraction of the applied voltage (85%) relative to the 5 V applied bias where $V_e \sim 2.8$ V (56%) in the same time and same temperature. Similar to the 5 V biasing, the time dependent V_e is roughly aligned with the logarithmic integrated charge density. Another measurement was performed at a higher temperature of 245 K biased with 3 V gate voltage, and the result is shown in Figure 3c. At this temperature the magnitude of I_g is much higher and it decays differently where a "bump" is observed. This behavior is likely due to the electrochemical etching, which has been reported by Shiogai *et al.*[20] Interestingly V_e does not appear to increase compared to that biased at 220 K. Either the viscosity change is not significant over this 25 K change or part of energy is consumed on etching instead of the EDL formation. Discoloration of the copper tape was observed in the 245 K measurement, which is noted in the optical micrograph (Fig. 3c inset) where the IL is cleaned off the tape. We note that the

calculated integrated charge density shown in Figure 2c is very high – values start at ~10^{-4} C/cm^2 to ~10^{-2} C/cm^2 during the 3-hour biasing at 220 K, which corresponds to ~10^{15} cm^{-2} to ~10^{17} cm^{-2} charge carriers, respectively. This is at least 2 orders of magnitude higher than the surface charge carrier densities reported.[1, 8, 23, 41] The higher integrated charges are attributed to multiple ion layers formed near the interface region[42, 43], though V_e is mostly affected by the ion layers that are closest to the IL-solid interface. Similar tests were performed using another popular IL, C_4mim-TF_2N, and the result can be found in supplementary materials Figure S1 and S2. The charging dynamics of different IL drop size was also conducted and the results are shown in Figure S3.

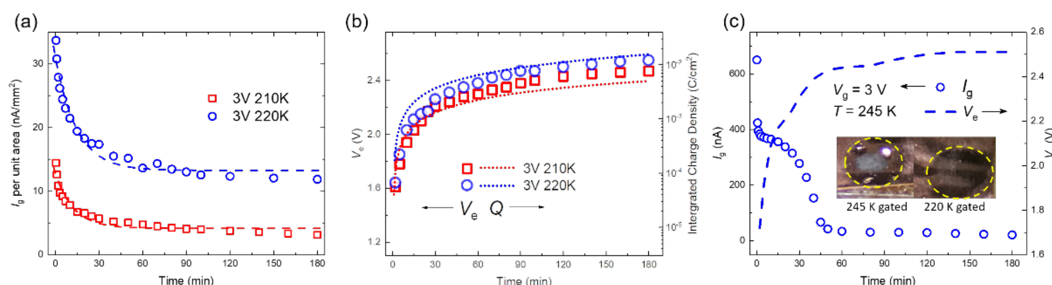

Figure 3. I_g and V_e in DEME IL monitored overtime with different applied gate voltage and temperature. With a lower V_g of 3 V, time dependent I_g and V_e is plotted in (a) and (b), respectively; note at 220 K with a lower I_g, V_e increases slower and yields at around 2.5 V after 3 hours. Dash lines in (a) are the exponential fittings of I_g, and dotted lines in (b) show the integration of I_g over time. (c) shows the result of the measurement with V_g = 3 V at 245 K; note the high current and an abnormal discontinuity in the I_g decay, which is likely due to electrochemical etching. Inset in (c) compares the optical images of 245 K biased area and 220 K biased area, where a noticeable etching effect at 245 K on copper tape is clearly seen. Yellow dashed circle indicates the area covered by IL droplets. The result of similar tests on another IL C_4mim-TF_2N can be found in the supplementary information.

To qualitatively investigate the charging dynamics, molecular dynamics simulations were performed on the [C_4mim][Tf_2N] IL and an Ag-Cu electrode system with implementation of constant potential method[32] to mimic the applied gate voltage. Figure 4a schematically illustrates the system of MD simulation, Figure 4b shows the atomic configuration of cation and anion, and Figure 4c is a plot of the surface charge density of the EDL at the (-) copper electrode as a function of time simulated at two potentials (3 V and 5 V) and three temperatures (210 K, 300 K, and 400 K). The cumulative charge density is solved via the Poisson equation by accounting for all the anion/cation layers relative to the metal surface. The dynamics of the EDL formation is characterized by the response of surface charge density, $Q(t)$, on the electrode surface and fitted by the exponential functions:

$$Q(t) = Q_{max}\left[1 - a exp^{-\frac{t}{b}} - (1-a) exp^{-\frac{t}{c}}\right] \quad (1)$$

where Q_{max} is the electrode surface charge density of the EDL in a pseudo-equilibrium and a, b are fitting parameters for the fast exponential and (1-a) and c are fitting parameters for the slow surface charging exponential (see Table S1 for a summary of the fitting parameters). Note for the 210 K

data, the dynamics are much slower and equilibrium is not reached, particularly for the 3 V data, during the 80 ns simulation time; however, the data fits reasonable well with equation 1. The initial clear trends that Figure 4(c) reveal are: 1) Q_{max} increases with increasing temperature, 2) for each temperature, higher voltage increases Q_{max}, and 3) increasing temperature and voltage increases the charging rate; all of these observations are are consistent with experiment. While the 210 K charge density is universally smallest and 5 V > 3V at all times, the 400 K-3 V condition initially charges faster than the 300 K-5 V condition ($b_{400K, 3V} = 0.412$ ns < $b_{300k, 5V} = 0.7586$ ns) at longer times (>10 ns) the 300 K-5 V condition has a higher surface charge density and ultimately a higher Q_{max}. Thus the simulations confirm what the experimental data revealed, namely, the surface charge density is a function of the applied voltage, temperature, and charging time.

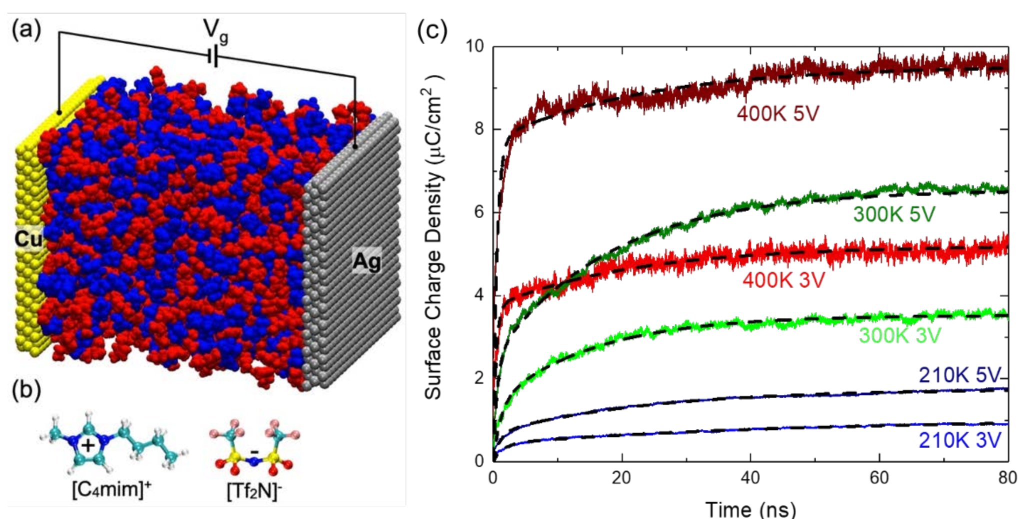

Figure 4. (a) Schematic illustrating the molecular dynamics simulation setup. (b) Atomic configuration of the $[C_4mim]^+$ cation and $[Tf_2N]^-$ anion. Time evolution of surface charge density under different temperatures (210, 300, and 400 K) and different gate voltage of (3 and 5 V). Note that in (c) the surface charge density is negative but shown its absolute value for clarity.

Figure 5 illustrates the number density as a function of position for the three temperatures for the $[C_4mim]^+$ cation (Fig. 5a,b) and the $[Tf_2N]^-$ anion (Fig. 5c,d) near the negatively charged copper electrode at $t = t_{max}$ for 3 V (Fig. 5a,c) and 5 V (Fig. 5b,d) (see Figure S4 for the ion distributions at the positive silver electrode). At 3 V the $[C_4mim]^+$ cations appear to have three dominant orientations with peaks at 0.29, 0.36 and 0.44 nm, while the first layer of $[Tf_2N]^-$ anions have peaks at 0.35, 0.40 and 0.49 nm. At 3 V the 0.29 nm peak is slightly higher at 300 K than 400 K, and the 0.36 nm peak is larger at 400 K than the 300 K orientation. Thus just based on the cation contribution, one expects the surface charge of the 300 K orientation to be higher. However, when one compares the $[Tf_2N]^-$ anion distribution, the 0.35 nm peak is also much higher at 300 K than 400 K, which counterbalances the cation charge density, and results in 400 K having a higher overall surface charge density. Similar arguments can be made for the 210 K-3 V condition; namely the overall $[C_4mim]^+$ cation density is slightly lower and has a higher total $[Tf_2N]^-$ anion density for the dominant orientations relative to 400 K. At 5 V the $[C_4mim]^+$ cation distributions at 0.29 nm increase for all temperatures and the overall $[Tf_2N]^-$ anion distribution shifts to longer distance relative to 3 V; both of which lead to higher overall surface charge density. While the specific ion distributions

and surface charge densities realized at the much longer and larger experimental conditions, the simulations illustrate that the total surface charge density is dependent on both the resultant anion and cation distributions; experimentally, these distributions are a function of the applied voltage, temperature, and charging time.

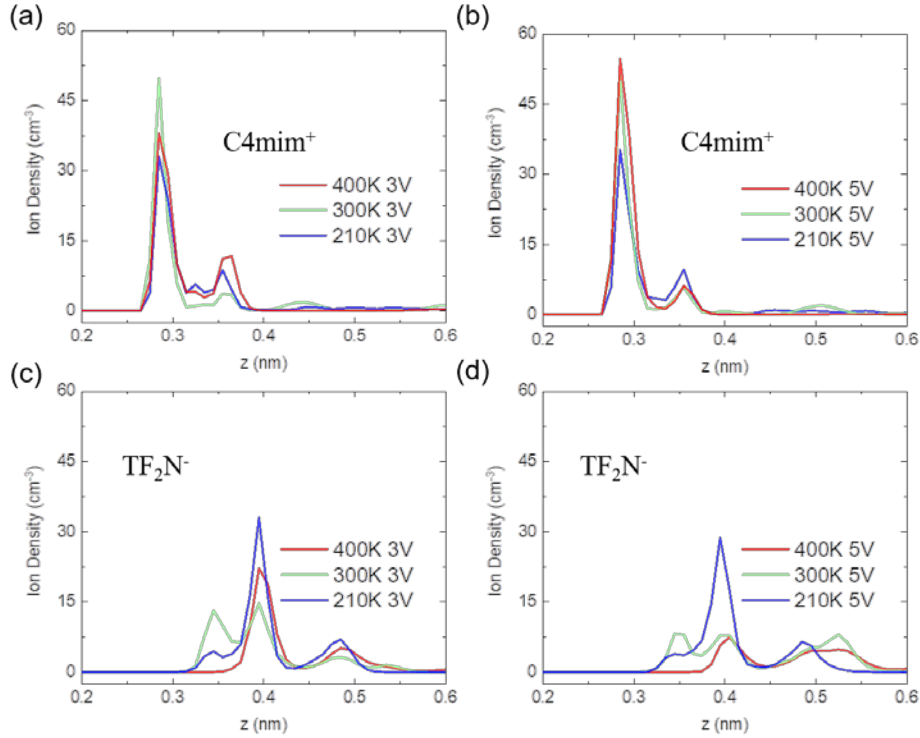

Figure 5. Number density as a function of distance for $t = t_{max}$ for ions near the copper electrode. (a) and (b) are for the $[C_4mim]^+$ cation, and (c) and (d) for the $[Tf_2N]^-$ anion. (a) and (c) are distributions under a 3 V gate bias and (b) and (d) are under a 5 V gate bias. z = 0 nm denotes the position of copper surface which is close to IL.

Based on the investigation above, we studied the IL biasing effect on FST films to establish the relationship between V_e and T_c. The film samples were prepared as described in the experimental section and illustrated in Fig. 6a). RT measurements as a function of V_e values are plotted in Figure 6b and 6c. At zero IL gate bias the FST film has a $T_c^0 = 17.8$ K and $T_c^{on} = 18.7$ K ,which is consistent with our previous reports.[31] Various V_e values were obtained by charging the EDL layer at certain applied gate voltages and times (see supplemental information for details); importantly during the RT measurements when T < 220, V_e remains essentially constant because below the glass transition temperature the EDL charging process is significantly slowed as the viscosity increases. As demonstrated in Figure 6b, the RT curves are not affected when $V_e < 1.67$ V. When V_e reaches 1.67 V a T_c enhancement is observed, as evidenced by the two-step superconducting transition. This indicates that only part of the channel layer is electrostatically doped and the superconducting phase starts to form at higher temperature; T_c^0, however does not change, indicating the superconducting phase is not continuous over the entire channel region. This two-step transition was also observed in previous IL biasing studies on FeSe.[16, 17, 20] As V_e is increased, the T_c^{on} is shifted to higher temperature and the T_c^0 remains unchanged until $V_e = 2.09$ V (see Fig. S5a for magnified view of

the low resistance region), where the 2-step transition disappears and a single transition is realized. At V_e = 2.16 V, the T_c^0 and T_c^{on} reaches the highest value of 30 K and 35 K, respectively. Further increase in V_e suppresses the T_c, which may indicate the film is over-doped. To test the reversibility superconducting properties, the applied gate bias was set to zero at 220 K after the test and the effective voltage was allowed to decay overnight. The T_c^0 and T_c^{on} recovered back to 18 K and 19 K, respectively, with a normal state resistance value similar to the initial measurement.

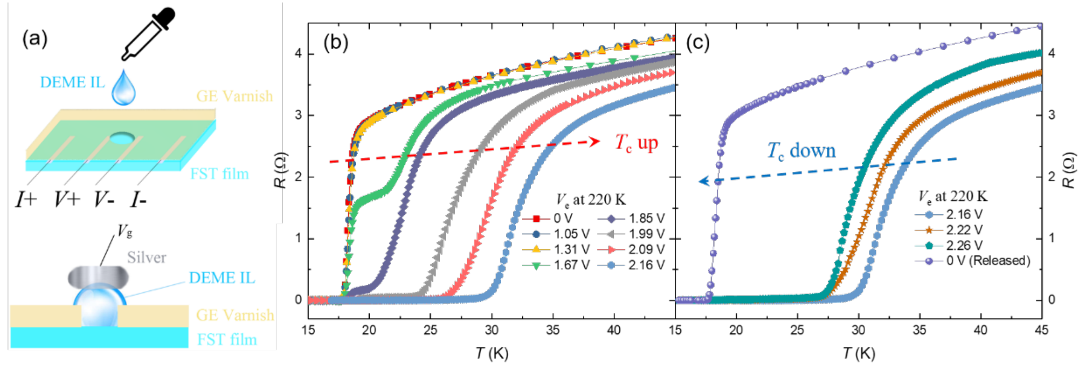

Figure 6. Temperature dependent resistance of FST film as a function of DEME IL equivalent voltages. Schematic illustrating the 4-point probe FST device used in R versus T measurements is shown in (a). The FST film with the DEME IL reservoir between the voltage leads is cooled down to 220 K before the gate bias was applied. The superconducting transition as a function of increasing V_e is shown in (b) and (c). T_c^0 and T_c^{on} of the pristine film are 17.8 K and 18.7 K, which increases up to 30 K and 35 K, respectively, as the V_e increases to 2.16 V. Higher V_e suppresses T_c, which is likely due to over-doping. After setting $V_g = 0$ bias overnight V_e drops to zero and T_c recovers back to its pristine value.

T_c enhancements of FeSe thin films and exfoliated single crystal flakes have been previously explored via DEME IL biasing. All previously reported enhancements were done on ultra-thin films/flakes with the thickness around or lower than 10 nm. Shiogai *et al* reported that T_c of FeSe films cannot be enhanced by biasing until being etched down to a few nm thick.[20] To confirm that our films were not electrochemically etched during the gate biasing, the biased film was focus ion beam (FIB) milled at multiple sites in the pristine and IL biased region, and subsequently imaged as shown in Figure 7a. The thickness of the biased film is ~140 nm, which is the same as the pristine film – no observable etching occurred during biasing. To confirm the layer identification, EDS line scans were performed along the thickness direction and the result of pristine and biased area is shown in Figure 7b and 7c, respectively. Fe and Zr was selected to indicate the FST film and the YSZ substrate, respectively.

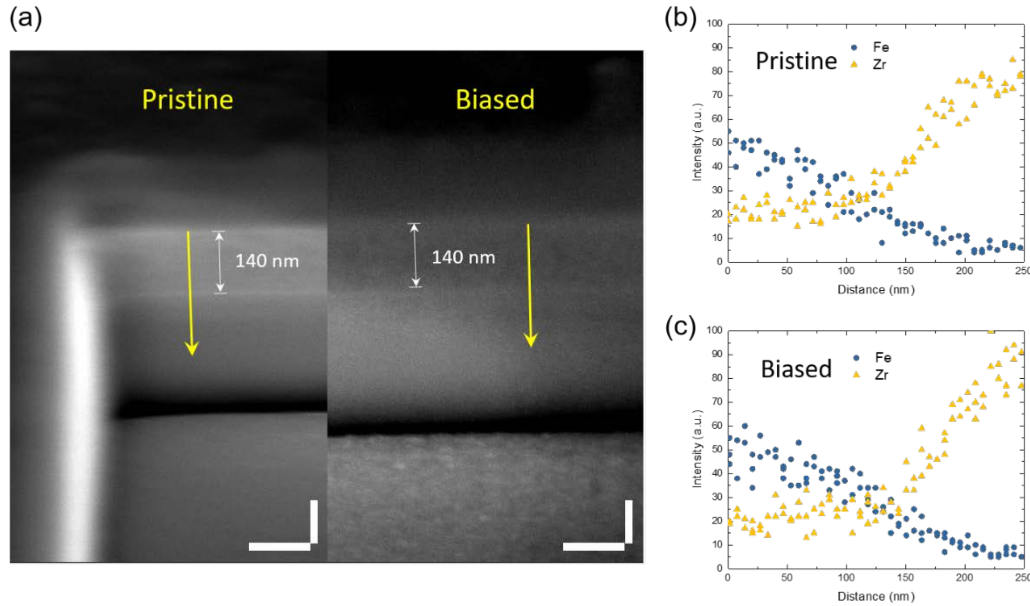

Figure 7. Tilted SEM image of the of pristine and biased area of a FST film, and EDS line scan along the thickness direction. A biased FST film was FIB milled and imaged in an SEM on a 45° tilted stage. The images compare a pristine and biased area of the film in (a), with no observable thickness change for the IL biased region. (b) and (c) are EDS line scans of Fe (film) and Zr (substrate) in pristine and biased areas, respectively, along the thickness direction (yellow arrow in (a)). White scale bars in (a) shows 100 nm length in horizontal and vertical directions.

Figure 7 confirms that the IL biasing process at 220 K does not etch the FST film. Compared to FeSe for which T_c IL biasing enhancements were only observed in ultra-thin film/flake, our study shows that this IL gating T_c enhancements areare applicable to > 100 nm thickness. While this could be due to intrinsic differences in FeSe versus FST, it could also be related to the EDL layer dynamics discussed above. Things are also complicated for ultrathin FeSe films approaching a few layers as interface effects or strain effects could also contribute to increasing higher T_c.[44, 45] Interestingly, while FST thin films have a higher intrinsic T_c than FeSe, the enhanced T_c due to IL biasing reaches the similar value of 35~40 K. It is reasonable to speculate that chemical doping and IL gating are complementary and that Te doping in FST contributes a partial chemical doping and the IL gating further electrostatically dopes the lattice. Note that the highest tunable T_c of FeSe gating is reported at ~48 K with a Li solid gate biasing[18], where the enhancing effect is attributed not only electrostatic doping but also the Li intercalation, which has been reported on other FET IL studies[6]. The highest T_c in FST is achieved at V_e = 2.16 V and we surmise that FeSe would need a higher V_e to electrostatically maximize its T_c value to 35 K. According to the low temperature EDL charging dynamics discussed above, V_e the effective IL bias is a strong function of temperature, applied voltage, and time. Thus, to elucidate the effects of electrostatic doping via IL gating at low temperature, significant care must be taken to clearly understand EDL dynamics.

Conclusion:

Low temperature dynamics of the ionic liquid electric double layer has been investigated. The state of the EDL are logically a function of gate voltage, time and temperature. At 210 K and 220 K long times are needed for the EDL to form in the ionic liquid. The concept of equivalent voltage V_e is introduced as a measure of the EDL formation during the low temperature biasing process. Molecular dynamic simulations were conducted and the results are qualitatively consistent with the experimental observation. To demonstrate the importance of understanding the charging dynamics, a 140 nm thick FST film was biased using the DEME IL and its onset T_c can be tuned from 18 to a maximum of 35 K for $0 \leq V_e \leq 2.16$ V, and apparently over-dopes when $V_e > 2.16$ V.

Acknowledgements

C.Z. and P.D.R. acknowledges support by U.S. Department of Energy (DOE) under Grant DE-SC0002136. W.B. acknowledges support from NSF (grant #1544686). $FeSe_{0.5}Te_{0.5}$ superconducting films were made at Brookhaven National Laboratory. Q.L. and G.G. were supported by the Office of Basic Energy Sciences, Division of Materials Sciences and Engineering, US Department of Energy under Contract No. DE-SC0012704. The authors also acknowledge that the device fabrication and electrical measurements were conducted at the Center for Nanophase Materials Sciences, which is a DOE Office of Science User Facility.

References

1. Nakano, M.; Shibuya, K.; Okuyama, D.; Hatano, T.; Ono, S.; Kawasaki, M.; Iwasa, Y.; Tokura, Y. *Nature* **2012,** 487, (7408), 459-462.
2. Ueno, K.; Nakamura, S.; Shimotani, H.; Ohtomo, A.; Kimura, N.; Nojima, T.; Aoki, H.; Iwasa, Y.; Kawasaki, M. *Nat. Mater.* **2008,** 7, (11), 855-858.
3. Jeong, J.; Aetukuri, N.; Graf, T.; Schladt, T. D.; Samant, M. G.; Parkin, S. S. P. *Science* **2013,** 339, (6126), 1402-1405.
4. UenoK; NakamuraS; ShimotaniH; Yuan, H. T.; KimuraN; NojimaT; AokiH; IwasaY; KawasakiM. *Nat. Nano.* **2011,** 6, (7), 408-412.
5. Kötz, R.; Carlen, M. *Electrochim Acta* **2000,** 45, (15), 2483-2498.
6. Zhang, C.; Pudasaini, P. R.; Oyedele, A. D.; Ievlev, A. V.; Xu, L.; Haglund, A. V.; Noh, J. H.; Wong, A. T.; Xiao, K.; Ward, T. Z.; Mandrus, D. G.; Xu, H.; Ovchinnikova, O. S.; Rack, P. D. *Acs Appl Mater Inter* **2018,** 10, (26), 22623-22631.
7. Ye, J. T.; Inoue, S.; Kobayashi, K.; Kasahara, Y.; Yuan, H. T.; Shimotani, H.; Iwasa, Y. *Nat. Mater.* **2010,** 9, (2), 125-128.
8. Yamada, Y.; Ueno, K.; Fukumura, T.; Yuan, H. T.; Shimotani, H.; Iwasa, Y.; Gu, L.; Tsukimoto, S.; Ikuhara, Y.; Kawasaki, M. *Science* **2011,** 332, (6033), 1065-1067.
9. Uesugi, E.; Goto, H.; Eguchi, R.; Fujiwara, A.; Kubozono, Y. *Sci. Rep.* **2013,** 3, 1595.
10. Black, J. M.; Come, J.; Bi, S.; Zhu, M.; Zhao, W.; Wong, A. T.; Noh, J. H.; Pudasaini, P. R.; Zhang, P.; Okatan, M. B.; Dai, S.; Kalinin, S. V.; Rack, P. D.; Ward, T. Z.; Feng, G.; Balke, N. *Acs Appl Mater Inter* **2017,** 9, (46), 40949-40958.
11. Leng, X.; Pereiro, J.; Strle, J.; Dubuis, G.; Bollinger, A. T.; Gozar, A.; Wu, J.; Litombe, N.;

Panagopoulos, C.; Pavuna, D.; Božović, I. *npj Quantum Materials* **2017,** 2, (1), 35.

12. Li, M.; Han, W.; Jiang, X.; Jeong, J.; Samant, M. G.; Parkin, S. S. P. *Nano Lett.* **2013,** 13, (10), 4675-4678.
13. Jeong, J.; Aetukuri, N. B.; Passarello, D.; Conradson, S. D.; Samant, M. G.; Parkin, S. S. P. *P. Natl. Acad. Sci. USA* **2015,** 112, (4), 1013-1018.
14. Altendorf, S. G.; Jeong, J.; Passarello, D.; Aetukuri, N. B.; Samant, M. G.; Parkin, S. S. *Adv. Mater.* **2016,** 28, (26), 5284-5292.
15. Ye, J. T.; Zhang, Y. J.; Akashi, R.; Bahramy, M. S.; Arita, R.; Iwasa, Y. *Science* **2012,** 338, (6111), 1193-1196.
16. Hanzawa, K.; Sato, H.; Hiramatsu, H.; Kamiya, T.; Hosono, H. *P. Natl. Acad. Sci. USA* **2016,** 113, (15), 3986-3990.
17. Lei, B.; Cui, J.; Xiang, Z.; Shang, C.; Wang, N.; Ye, G.; Luo, X.; Wu, T.; Sun, Z.; Chen, X. *Phys. Rev. Lett.* **2016,** 116, (7), 077002.
18. Lei, B.; Wang, N. Z.; Shang, C.; Meng, F. B.; Ma, L. K.; Luo, X. G.; Wu, T.; Sun, Z.; Wang, Y.; Jiang, Z.; Mao, B. H.; Liu, Z.; Yu, Y. J.; Zhang, Y. B.; Chen, X. H. *Phys. Rev. B* **2017,** 95, (2), 020503.
19. Lei, B.; Xiang, Z.; Lu, X.; Wang, N.; Chang, J.; Shang, C.; Zhang, A.; Zhang, Q.; Luo, X.; Wu, T. *Phys. Rev. B* **2016,** 93, (6), 060501.
20. Shiogai, J.; Ito, Y.; Mitsuhashi, T.; Nojima, T.; Tsukazaki, A. *Nat. Phys.* **2016,** 12, (1), 42-46.
21. Bollinger, A. T.; Dubuis, G.; Yoon, J.; Pavuna, D.; Misewich, J.; Božović, I. *Nature* **2011,** 472, (7344), 458.
22. Ueno, K.; Shimotani, H.; Yuan, H.; Ye, J.; Kawasaki, M.; Iwasa, Y. *J. Phys. Soc. Jpn.* **2014,** 83, (3), 032001.
23. Ye, J.; Inoue, S.; Kobayashi, K.; Kasahara, Y.; Yuan, H.; Shimotani, H.; Iwasa, Y. *Nat. Mater.* **2010,** 9, (2), 125.
24. Ozaki, T.; Wu, L.; Zhang, C.; Jaroszynski, J.; Si, W.; Zhou, J.; Zhu, Y.; Li, Q. *Nat. Commun.* **2016,** 7, 13036.
25. Zhang, C.; Si, W.; Li, Q. *Appl. Phys. Lett.* **2016,** 109, (20), 202601.
26. Sun, Y.; Taen, T.; Tsuchiya, Y.; Shi, Z. X.; Tamegai, T. *Superconductor Science and Technology* **2013,** 26, (1), 015015.
27. Li, Q.; Si, W.; Dimitrov, I. K. *Rep. Prog. Phys.* **2011,** 74, (12), 124510.
28. Liu, T. J.; Hu, J.; Qian, B.; Fobes, D.; Mao, Z. Q.; Bao, W.; Reehuis, M.; Kimber, S. A. J.; Prokeš, K.; Matas, S.; Argyriou, D. N.; Hiess, A.; Rotaru, A.; Pham, H.; Spinu, L.; Qiu, Y.; Thampy, V.; Savici, A. T.; Rodriguez, J. A.; Broholm, C. *Nat. Mater.* **2010,** 9, (9), 718-720.
29. Si, W.; Lin, Z.-W.; Jie, Q.; Yin, W.-G.; Zhou, J.; Gu, G.; Johnson, P. D.; Li, Q. *Appl. Phys. Lett.* **2009,** 95, (5), 052504.
30. Si, W.; Zhou, J.; Jie, Q.; Dimitrov, I.; Solovyov, V.; Johnson, P. D.; Jaroszynski, J.; Matias, V.; Sheehan, C.; Li, Q. *Appl. Phys. Lett.* **2011,** 98, (26), 262509.
31. Si, W.; Han, S. J.; Shi, X.; Ehrlich, S. N.; Jaroszynski, J.; Goyal, A.; Li, Q. *Nat. Commun.* **2013,** 4, 1347.
32. Bi, S.; Wang, R.; Liu, S.; Yan, J.; Mao, B.; Kornyshev, A. A.; Feng, G. *Nat. Commun.* **2018,** 9, (1), 5222-5222.
33. Péan, C.; Merlet, C.; Rotenberg, B.; Madden, P. A.; Taberna, P.-L.; Daffos, B.; Salanne, M.; Simon, P. *ACS Nano* **2014,** 8, (2), 1576-1583.

34. Canongia Lopes, J. N.; Pádua, A. A. *J. Phys. Chem. B* **2004,** 108, (43), 16893-16898.
35. Heinz, H.; Vaia, R. A.; Farmer, B. L.; Naik, R. R. *J. Phys. Chem. C* **2008,** 112, (44), 17281-17290.
36. Hess, B.; Kutzner, C.; van der Spoel, D.; Lindahl, E. *Journal of Chemical Theory and Computation* **2008,** 4, (3), 435-447.
37. Hess, B.; Bekker, H.; Berendsen, H. J.; Fraaije, J. G. *J. Comput. Chem.* **1997,** 18, (12), 1463-1472.
38. Bussi, G.; Donadio, D.; Parrinello, M. *J. Chem. Phys.* **2007,** 126, (1), 014101.
39. Raghunathan, A. V.; Aluru, N. R. *Physical Review E* **2007,** 76, (1), 011202.
40. Si, W.; Zhang, C.; Shi, X.; Ozaki, T.; Jaroszynski, J.; Li, Q. *Appl. Phys. Lett.* **2015,** 106, (3), 032602.
41. Fedorov, M. V.; Kornyshev, A. A. *Electrochim Acta* **2008,** 53, (23), 6835-6840.
42. Ivaništšev, V.; Fedorov, M. V. *The Electrochemical Society Interface* **2014,** 23, (1), 65-69.
43. Bazant, M. Z.; Storey, B. D.; Kornyshev, A. A. *Phys. Rev. Lett.* **2011,** 106, (4), 046102.
44. Bellingeri, E.; Kawale, S.; Braccini, V.; Buzio, R.; Gerbi, A.; Martinelli, A.; Putti, M.; Pallecchi, I.; Balestrino, G.; Tebano, A.; Ferdeghini, C. *Superconductor Science and Technology* **2012,** 25, (8), 084022.
45. Ge, J.-F.; Liu, Z.-L.; Liu, C.; Gao, C.-L.; Qian, D.; Xue, Q.-K.; Liu, Y.; Jia, J.-F. *Nat. Mater.* **2015,** 14, (3), 285.

Supplementary Materials

Low Temperature Charging Dynamics of Ionic Liquid and Its Gating Effect on FeSe0.5Te0.5 Superconducting Films

Cheng Zhang[1,2], Wei Zhao[3], Sheng Bi[3], Christopher M. Rouleau[2], Jason D. Fowlkes[2], Walker Boldman[1], Genda Gu[4], Qiang Li[4], Guang Feng[3], and Philip D. Rack[1,2,]*

[1] Department of Materials Science and Engineering, University of Tennessee, Knoxville, Tennessee 37996, USA

[2] Center for Nanophase Materials Sciences, Oak Ridge National Laboratory, Oak Ridge, Tennessee 37831, USA

[3] State Key Laboratory of Coal Combustion, School of Energy and Power Engineering, Huazhong University of Science and Technology (HUST), Wuhan 430074, China

[4] Department of Condensed Matter Physics and Materials Science, Brookhaven National Laboratory, Upton, New York 11973, USA

***prack@utk.edu**

Figure S1. Time dependent I_g and V_e in C4mim IL with an applied gate voltage of 5 V, measured at 220 K and 210 K. The current density, normalized based on the droplet projected area, as a function of time is plotted in (a), with the exponential decay fittings in dash lines. The measured V_e as a function of time is shown in (b). The exponential decay of I_g and rise of V_e are qualitatively similar to the DEME IL.

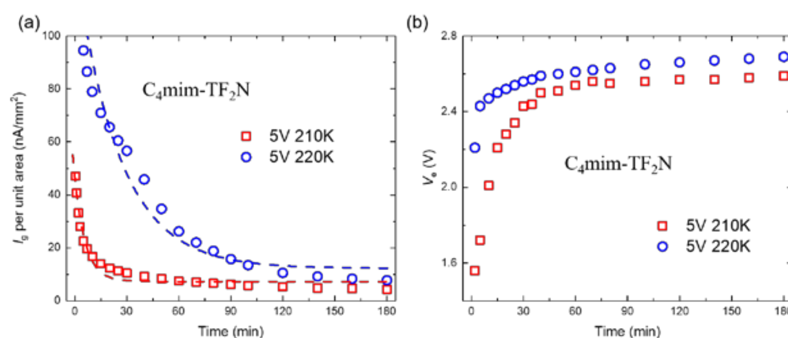

Figure S2. Time dependent I_g (a) and equivalent voltage V_e (b) in C4mim IL with an applied gate voltage of 3 V, measured at 220 K and 210 K. Similar as the DEME IL, 3 V biasing leads to lower current flow and slower V_e charging. Dash lines in (a) are exponential decay fittings. (c) is the result of I_g and V_e measured under 245 K with 3 V applied gate. We note an electrochemical reaction also happens at 245 K when using C4mim on Cu tape. Yellow dashed circle indicates the area covered by IL droplets

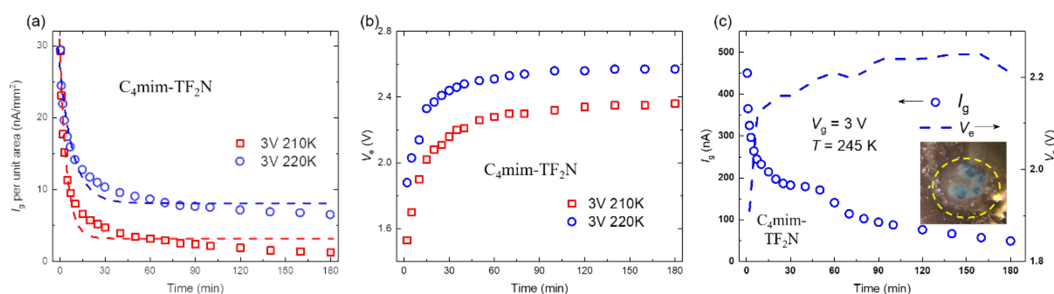

Figure S3. Investigation of IL droplet size effect using DEME under applied gate voltages of 3 V (a)(b) and 5 V (c)(d) at 220 K. Time dependent I_g and V_e curves of large and small IL droplets were measured. Large droplets leads to higher I_g, while curves of normalized I_g per unit area against time almost overlap as shown in insets of (a) and (c). The droplet size effect on V_e is also very small.

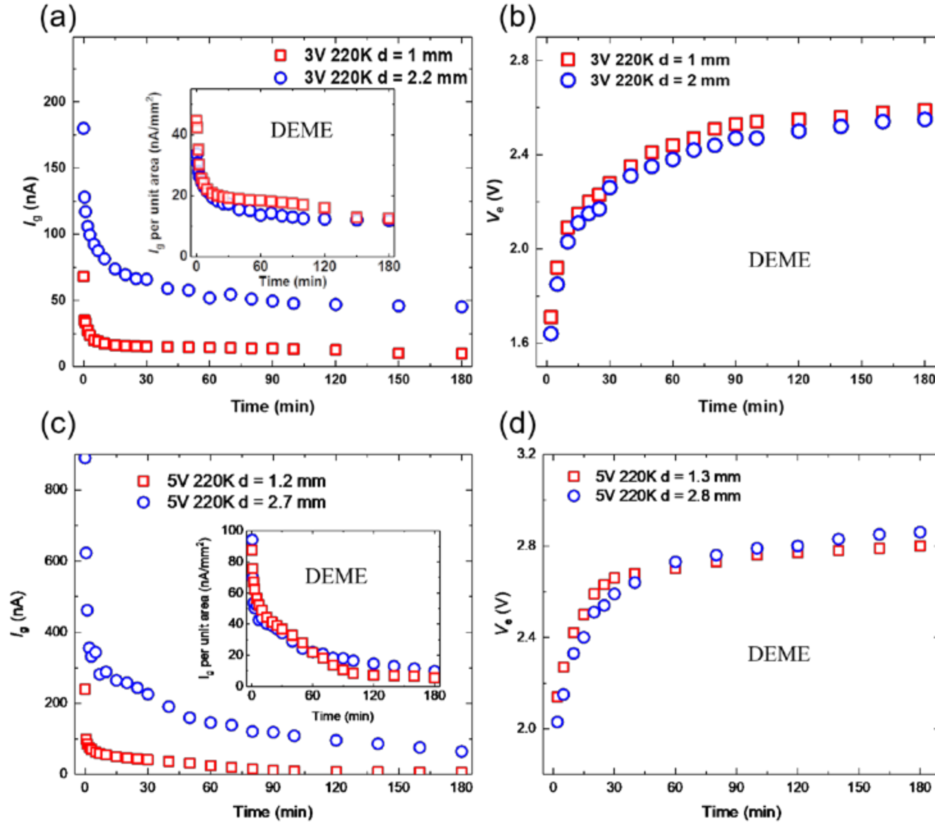

Table S1. Fitting parameters for the fits to the MD surface charge density versus time plots.

Temp.	Bias	Q_{max} (μC cm^{-2})	a	b (ns)	c (ns)	R^2
210K	3V	1.027	0.413	1.444	45.32	0.9903
	5V	1.752	0.3912	1.018	23.82	0.9924
300K	3V	3.498	0.3657	1.008	14.27	0.985
	5V	6.724	0.3991	0.7586	21.35	0.9959
400K	3V	5.121	0.71	0.4122	17.44	0.9263
	5V	9.788	0.8087	0.6347	35.18	0.9218

Figure S4. Number density as a function of distance for $t = t_{max}$ for (a) and (b) the $[C_4mim]^+$ cation and (c) and (d) the $[Tf_2N]^-$ anion near the silver electrode. (a) and (c) are distributions under a 3 V gate bias and (b) and (d) are under a 5 V gate bias. z = 8 nm denotes the position of silver surface which is close to IL.

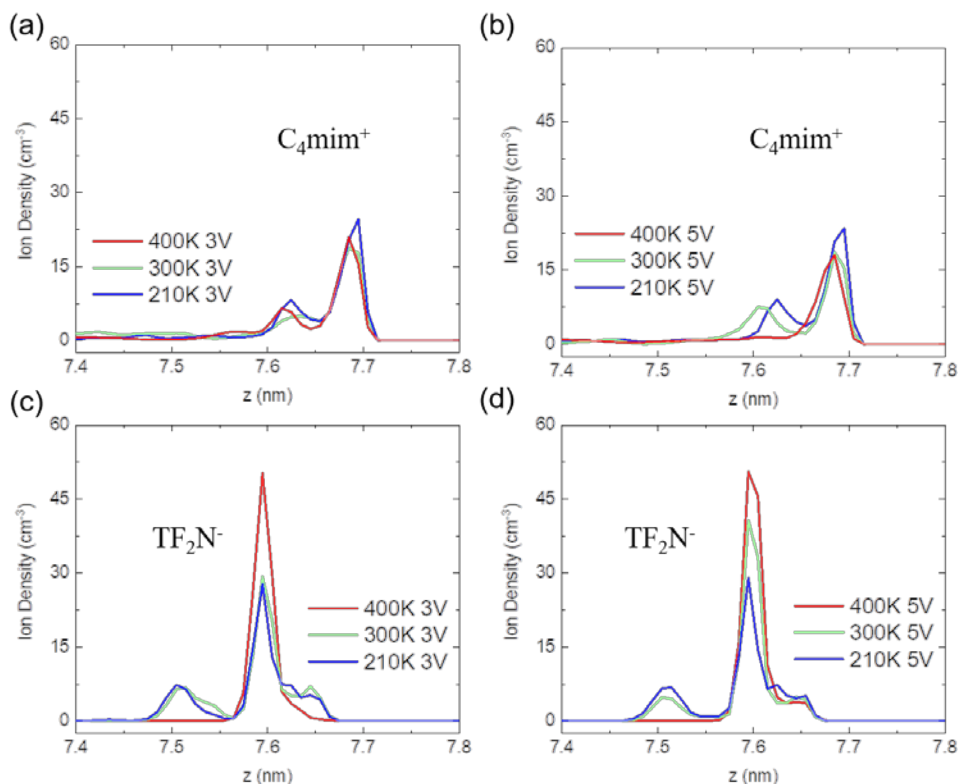

Figure S5. (a) Temperature dependent normalized resistance of FST film as a function of DEME IL equivalent voltages, zoomed in the low resistance region. The two-step transition with enhanced T_c^{on} and low T_c^0 disappears V_e reached 2.09 V. Extrapolation method is used to determine the T_c, as shown in (b) and (c) for $V_e = 0$ V and $V_e = 2.16$ V. T_c^0 and T_c^{on} can be enhanced from 17.9 K and 18.7 K to 30 K and 35 K, respectively, by DEME IL gating.